Impact of HVDC Dynamic Modelling on Power System Small Signal Stability Assessment

Impact of HVDC Dynamic Modelling on Power System Small Signal Stability Assessment

Surat Asvapoositkul, Robin Preece

Department of Electrical and Electronic Engineering, the University of Manchester, Manchester M13 9PL, U.K.

Abstract

This paper presents a new measure that can be used to identify the locations where high levels of HVDC modelling can be simplified while maintaining the accuracy of the small-signal stability results. Low-frequency inter-area oscillations have posed a major issue to power system operations and stability, for example by reducing the maximum power transfer on tie lines connected between different regions or causing cascading failure due to ever-growing oscillations. In modern power systems, a significant number of High Voltage Direct Current (HVDC) systems are connected to power networks. An appropriate level of HVDC modelling is required in order to obtain accurate small-signal stability results in multi-infeed HVDC systems. Although accurate results can be obtained by using complex modelling details, this can be prohibitively computationally expensive due to increasing simulation time. In this paper, different levels of modelling fidelity for HVDC systems are investigated in order to establish the impact of the included HVDC system dynamics on small-signal stability. It is shown that some dynamic HVDC modelling, particularly LCC-HVDC and VSC-HVDC with *P*-*Q* control, can be replaced by simplified models in order to reduce the simulation time and model complexity while maintaining the accuracy of small-signal stability results. Furthermore, a method to identify which HVDC systems require detailed modelling based on the quantification of changes to critical mode shapes is developed.

Keywords: Electromechanical oscillations, HVDC, Modelling, Power system dynamics, Small-signal stability.

1. Introduction

Several renewable energy sources (RES), such as wind and solar energy, are connected to the grids through power electronics due to significant development in power electronics technology and reduced cost of capital. The European Union has set a new binding target of 32% energy consumption from renewable energy by 2030, which is 5% higher than the original plan [1]. In the UK, the electricity generation from renewable energy increased 230% from 2009 to 2016 [2]. The UK government has set a target to deliver 30 GW of generating capacity from offshore wind by 2030 [3]. Typically, HVDC transmission systems have been connected to large-scale offshore wind farms or other power systems in order to facilitate access to the grid, improve security of supply in electricity and create new opportunities for electricity market. In 2016, the global installed capacity of HVDC interconnectors was approximately 270 GW [4]. More than 200 HVDC systems were operating in 2018 and a large number of HVDC projects are in planning or development stages [5]. It is expected that the global installed capacity of HVDC will be approximately 540 GW by 2025 [4].

The stability of mixed AC/DC systems needs to be investigated since a significant number of power electronics (PE) interfaced devices have been integrated to power systems [6]. Low-frequency electromechanical oscillations, particularly inter-area oscillations, are one of the major concerns in large interconnected power systems. These oscillations may limit the power transfer capability between different areas or, in the worst case, cause severe outages due to undamped oscillations [7], [8]. One such poorly-damped inter-area oscillation is found in the Great Britain (GB) network. This results from the oscillation between a group of generators in Scotland against a group of generators in England. The low-frequency oscillation has been identified as a main factor for the limited power transfer between Scotland and England [9]. In modern power systems, it is common to have several HVDC systems connected to the grid in close proximity, forming multi-infeed HVDC systems. However, with an ever-increasing number of HVDC connections, the modelling complexity grows rapidly. Due to the fast time-constants associated with HVDC converters and their controls, this can lead to significant issues with respect to the computational burden of simulation-based stability studies.

Modelling a PE-interfaced source, including an HVDC system, as a static load is of significant convenience as it reduces the modelling complexity and computational burden of simulations. For this reason, it is an often-used approach in many large-scale power system studies [10], [11]. However, it cannot reflect the dynamic characteristics of an HVDC system. For example, the responses of LCC-HVDC systems following a temporary disturbance are controlled based on the threshold values of the AC and DC voltage at the converter terminals [12]. In VSC-HVDC systems, different controls in the dynamic model will result in different transient responses, even for similar disturbances [13]. The AC transient propagation through a VSC-HVDC connection is studied in [14]. The study shows that the AC dynamic transient can propagate unidirectionally from the VSC with active power control to the VSC with DC voltage control while the AC transient can propagate bidirectionally between the VSCs with DC voltage control. Thus, dynamic modelling of both LCC-HVDC and VSC-HVDC systems has a better accuracy for studying system-level transient than modelling an HVDC system as a static load [15]. However, it is computationally expensive and significant time for simulations is inevitable.

Impacts of different control modes in LCC-HVDC and VSC-HVDC systems on small-signal stability have been investigated many times, for example in [16] and [17]. The impacts of a phase-locked loop (PLL) and control strategies at the inverter station of LCC-HVDC system on small-signal stability are investigated in [16]. The study shows that an increasing in PLL gain can cause the small-signal instability. Furthermore, under the same PLL setting, constant voltage control provides better damping of the dominant mode, compared to constant extinction control [16]. The impacts of different reactive power control strategies in VSC-HVDC system on small-signal are studied in [17]. The study shows that the VSC-HVDC with P-V_{ac} control mode can provide better stability in weak AC grids, compared to P-Q control, since it can adjust reactive power in order to maintain the desired voltage [17].

The small-signal stability under different control modes in multi-infeed VSC-HVDC and hybrid multi-infeed HVDC (H-MIDC), having both LCC and VSC technologies, is investigated in [18], [19]. The impact of reactive power control and AC voltage control in multi-infeed system is investigated in [18]. The results indicate that even though the AC voltage control can provide damping to some system modes, it may significantly reduce the damping of the least damped oscillatory mode. The analysis of small-signal stability in a H-MIDC system shows that three parameters in H-MIDC,

including the PLL gain of the LCC, the PLL gain of the VSC, and the proportional gain of the AC voltage control in the VSC, play an important role in system damping. Values of these parameters which are too large will deteriorate the damping of the dominant mode. Therefore, small values of PLL gains, within an acceptable range, are preferable [19]. Several studies have investigated the impacts of different control modes in both single and multi-infeed HVDC systems on small signal-stability. However, the impacts of different control modes on inter-area oscillations are not well addressed since most studies are conducted on small-test systems. The main limitation is that the analysis of inter-area oscillations inherently requires large power system models – inevitably resulting in complex power system modelling. Therefore, comparative analysis between different HVDC modelling complexities on small-signal stability has not been well addressed, which is the main focus of this paper. By replacing the complex modelling of electrical equipment while maintaining the accuracy of the results, larger power systems can be constructed and many other studies of power system stability can be conducted.

The objective of this paper is to identify the required level of dynamic HVDC modelling in order to achieve accurate stability assessment in complex mixed AC/DC systems. This will present the trade-off between the accuracy of dynamic responses and the complexity of the HVDC dynamic models. In this paper, the impacts of different modelling details of HVDC systems, both static and dynamic modelling, on small-signal stability are investigated in a complex mixed AC/DC system containing a significant proportion of HVDC and PE-interfaced sources. The critical system eigenvalues obtained under different modelling assumptions are compared in order to identify the necessary modelling fidelity required. The main contributions of this research are summarized as follows:

- Damping ratios between different levels of modelling detail are compared over a wide range of operating scenarios in order to investigate the trade-off between the accuracy of damping assessment and the complexity of HVDC modelling.
- A new measure has been developed that quantifies changes in mode shapes as modelling detail is changed. This index is used to show the impact of including detailed dynamic HVDC models on a critical mode shape, and therefore to identify priority locations where high levels of model detail are required.

The remainder of the paper is organised as follows. Different modelling details of HVDC systems, both LCC-HVDC and VSC-HVDC are outlined in Section 2. A brief summary of small-signal stability analysis is presented in Section 3. The proposed methodology for a new quantitative measure based on mode shape analysis is explained in Section 4. In Section 5, modelling details and modelling consideration of the test system are discussed. A thorough investigation on the performance and reliability of the proposed quantitative index is provided in Section 6. Finally, Section 7 provides the conclusions and areas of future research.

2. Modelling of HVDC Systems

As the adequacy of modelling complexity for small-signal stability is investigated in this study, two different levels of modelling detail of HVDC systems have been used, including simplified HVDC modelling [10] and dynamic average-value modelling (AVM) of an HVDC system [20], [21]. Full detailed modelling is not considered in this study because the effects of switching and harmonics in the HVDC converters are typically neglected for small-signal stability studies [22].

2.1. Simplified modelling of HVDC systems

Typically, offshore wind generation is connected to the grid through PE-interfaced devices. Wind generation has been considered as a negative load connected to the system in many large-scale power system studies [10], [11]. Therefore, in this study, HVDC systems, both Line Commutated Converter (LCC) and Voltage Source Converter (VSC), will be considered as two constant power loads connected on the rectifier and inverter sides. The positive power load is connected to the sending end, bus *i*, to represent the power being absorbed from the grid to the DC system. The negative power load is connected to the receiving end, bus *j*, to represent the power being injected from the DC system to the AC system. The losses in the DC line are neglected. Therefore, the relationship between active power at sending and receiving end can be described as $P_i = -P_j$. The simplified injection model is shown in Figure 1.

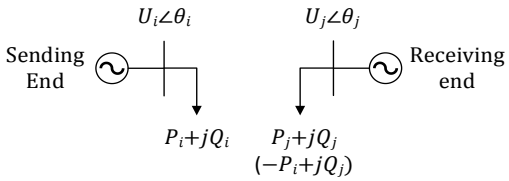

Figure 1. Simplified injection model of an HVDC system

In Figure 1, subscript *i* and *j* represent sending and receiving end buses. *U* and θ represent AC voltage magnitude and voltage angle respectively. *P* and *Q* are active and reactive power injected or absorbed at each bus.

2.2. Dynamic Modelling of HVDC Systems

Aspects of the dynamic modelling of HVDC systems, both LCC-HVDC and VSC-HVDC, are explained in this section. The dynamic modelling of HVDC systems has been implemented in this study to represent the transient behaviour and steady-state characteristics of HVDC systems in the system-level stability studies [15]. The effects of switching and harmonics are neglected since only small-signal stability is considered. Note that the dynamic modelling of HVDC systems is covered extensively in [20], [21]. Only aspects relevant to the subsequent results obtained are included.

2.2.1 LCC-HVDC Model

For LCC-HVDC systems, the DC voltages at both rectifier and inverter sides are controlled by varying the firing angle. The DC current can be manipulated by varying the DC voltage at either rectifier side or inverter side [20]. The calculation of DC voltage at both rectifier and inverter sides as well as DC current can be expressed as (1)-(3).

$$V_{dcr} = B\frac{3\sqrt{2}}{\pi}\mathrm{V_{g\_LLr}}\cos\alpha_r - B\frac{3}{\pi}\omega L_{tr}I_{dc} \tag{1}$$

$$V_{dci} = B\frac{3\sqrt{2}}{\pi}\mathrm{V_{g\_LLi}}\cos\beta + B\frac{3}{\pi}\omega L_{ti}I_{dc} \tag{2}$$

$$I_{dc} = \frac{V_{dcr} - V_{dci}}{R_{dc}} \tag{3}$$

In (1)-(3), subscript *r* and *i* stand for rectifier and inverter. V_{dc} and I_{dc} are DC voltage and DC current respectively. V_{g_LL} is the line-line RMS converter voltage. B is the number of bridges connected in series, B = 2 for 12-pulse converter and B = 4 for 24-pulse converter. α is the firing angle and β is ignition advance angle. L_t is a commutation inductance and R_{dc} is total DC-side resistance. The overview of the control system of a LCC-HVDC system is shown in Figure 2. The dynamic LCC-HVDC model used in this simulation is equivalent to the CDC4T model developed in PSS/E [23]

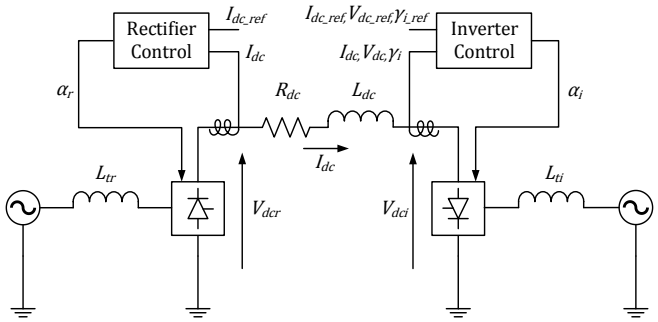

Figure 2. LCC-HVDC configuration

In Figure 2, subscript *ref* stands for a reference value of specified signals. L_{dc} is total-DC side reactance and γ is an extinction angle. The DC line in the dynamic LCC-HVDC model is represented as a series lumped R-L circuit. This lumped R-L line modelling is implemented since the full frequency response and all electric field effects can be neglected for small-signal stability studies [24].

2.2.2 Control Strategies of LCC-HVDC Systems

In the typical control strategy of LCC-HVDC converters, a DC current control mode is employed at the rectifier side while current control, gamma control and Voltage Dependent Current Order Limiter (VDCOL) are used in the control of the inverter [25]. The Constant Current Control (CCC) technique is implemented in the rectifier control as shown in Figure 3 [20]. The reference current order (I_{dc_ref}) is obtained by comparing between the DC current order from VDCOL and the desired DC current from DC power dispatch (P_{ref}). The minimum of the two is selected as a reference current order for rectifier control.

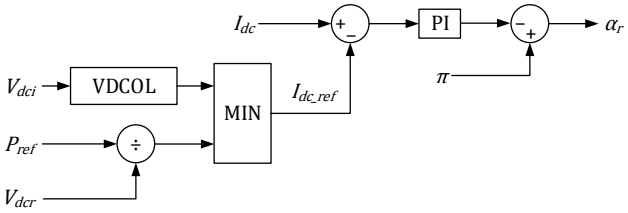

Figure 3. Rectifier DC current control

The inverter control can be performed through different control approaches, consisting of DC current control, DC voltage control and extinction angle (γ) control (EAC) modes as shown in Figure 4 [20]. In the DC current control mode, the reference signal is obtained as for the rectifier control. However, unlike the DC current control in the rectifier, the DC current in the inverter is controlled to the value of reference current order minus current margin ($I_{dc\_ref} - I_{margin}$). The current margin is

introduced to the inverter current control to manipulate the power reversal process [26]. The current margin is typically set to 0.1-0.15 pu. It is common to introduce a current error control (CEC) signal between the DC current control and DC voltage. This CEC can also be introduced between the DC current control and extinction angle control in order to make transitions between different control modes more smooth [27], [28]. The minimum of these signals is selected as the inverter control mode because it is desirable to operate the inverter at the minimum extinction angle to minimise reactive power consumption, power losses and harmonic level [20].

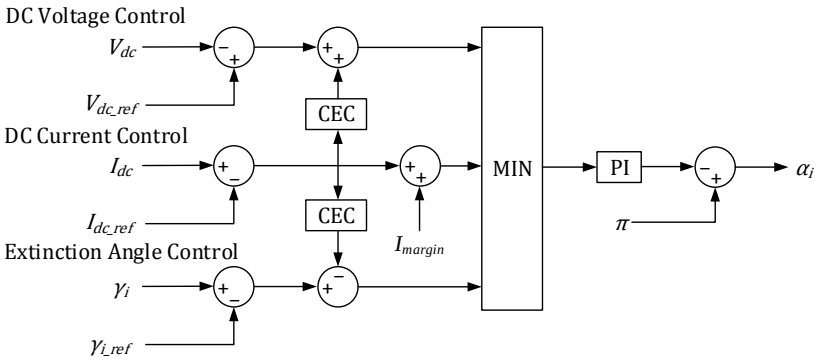

Figure 4. Inverter DC current control, DC voltage control and EAC control

2.2.3 VSC-HVDC Model

The VSC-HVDC technology has many advantages over the LCC-HVDC such as independent control of active and reactive power, less harmonic content and black-start capability [20]. In this paper, the half-bridge Modular Multilevel Converter (MMC) configuration is considered. A half-bridge MMC VSC-HVDC system consists of an array of sub-modules, SMs, connecting in series in each converter arm as shown in Figure 5. Each sub-module contains half-bridge converter with two IGBTs and one parallel capacitor [20]. A dynamic model of a half-bridge MMC-HVDC system is constructed based on the CIGRE guidelines [21]. The dynamic AVM of a VSC-HVDC does not include the effects of switching, harmonics and energy balancing [15].

The operation in each sub-module is similar to two-level half-bride converter, connecting or bypassing a sub-module. When the sub-module is connected, the output voltage (V_{sm}) equals to capacitor voltage. When the sub-module is by-passed, the output voltage is zero. A desired AC voltage waveform is built by sequentially switching series-connected sub-modules [29]. The phase voltages at the AC converter terminal can be controlled by varying the voltages at the upper and lower arms [30]. The converter phase voltage can be calculated as expressed in (4).

$$V_a = \frac{V_{la} - V_{ua}}{2} - \frac{L_{arm}}{2}\frac{dI_a}{dt} - \frac{R_{arm}}{2}I_a \tag{4}$$

In (4), V_a and I_a are the converter phase voltage and current respectively. V_{ua} and V_{la} are the upper arm and lower arm voltages. R_{arm} and L_{arm} are resistance and inductance in each converter arm.

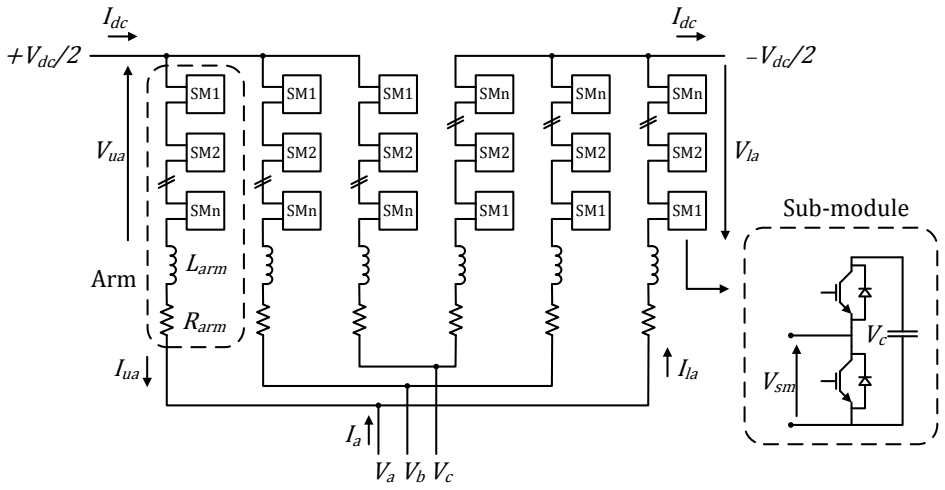

Figure 5. Three-phase half-bridge MMC [30]

In Figure 5, subscript *a*, *b* and *c* stand for phase A, B and C in the AC system. R_{arm} and L_{arm} are resistance and inductance in each converter arm. In this study, the DC line connected between the two converters is modelled as an equivalent π-circuit since full frequency analysis is not performed.

2.2.4 Control Strategies of VSC-HVDC Systems

The control schemes of interest of VSC-HVDC for power system dynamic assessment consist of the inner current control and outer control. The inner current control uses fast decoupled current control, known as DQ current control, in order to achieve the fast response and to ensure the protection and stability of the converter. The cross coupling between d-axis and q-axis in the inner current control has only an extremely small impact on the inter-area oscillations. This is due to the significant difference in the bandwidth of the inner current control (approximately 1000 Hz) and the frequency of inter-area oscillations (0.25-1 Hz) [20]. The outputs of the inner control are pulse-width modulation indices in the d-axis (P_{md}) and q-axis (P_{mq}). The outer control is implemented to achieve the system performance objectives. The outputs of the outer control are sent as reference signals to the inner current control in d-axis (I_{d_ref}) and q-axis (I_{q_ref}) [20]. The reference signals then are compared with the converter current in d-axis (I_d) and q-axis (I_q). Four types of outer control, including active power control, reactive power control, DC voltage control and AC voltage control, are considered within this work. Further control schemes (such as AC voltage and frequency control) may be considered for islanded system operation. The two-level cascaded control of VSC-HVDC systems is shown in Figure 6.

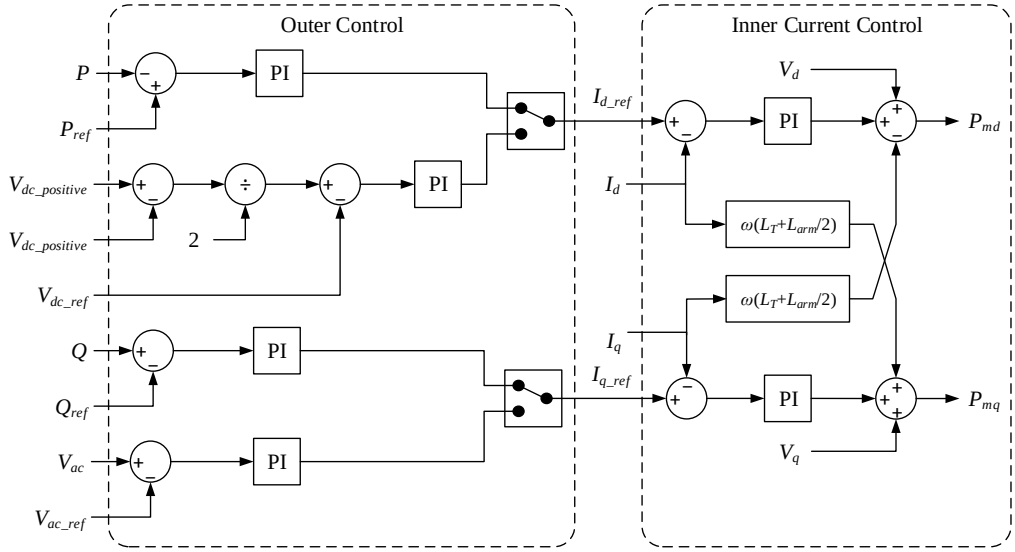

Figure 6. Block diagrams of outer control

In Figure 6, P and P_{ref} are the actual and reference active power delivered at the converter terminal. Q and Q_{ref} are the actual and reference reactive power delivered at the converter terminal. $V_{dc\_positive}$, $V_{dc\_negative}$ and V_{dc_ref} are DC voltage at the positive DC bus, negative DC bus and the reference DC voltage respectively. V_{ac} and V_{ac_ref} are AC voltage at the converter AC terminal and the reference AC voltage. V_d and V_q are the voltage at the converter terminal in d-axis and q-axis respectively. L_T and L_{arm} are the converter transformer reactance and arm reactance of the MMC.

Although the different HVDC modelling can provide identical active power, reactive power and AC voltage at the connection point, the control strategies inside the HVDC models are totally different. Control strategies under different HVDC modelling fidelity during dynamic operation are summarised in Table 1.

Table 1: Control strategies for different HVDC modelling

Control variables	Simplified HVDC model	Dynamic LCC-HVDC model	Dynamic VSC-HVDC model
Active Power	Directly sets active power in constant power load	DC current control at rectifier DC current, DC voltage or gamma control at inverter	Active power or DC voltage control in d-axis
Reactive Power	Directly sets reactive power in constant power load	No reactive power control. Desired reactive power is obtained by adjusting shunt elements at the HVDC terminal.	Reactive power or AC voltage control in q-axis

3. Small-Signal Stability

Small-signal stability is the ability to maintain stability of an electrical power system after being subjected to small perturbations [31]. The small disturbances can be considered sufficiently small to allow nonlinear equations in power systems to be linearised around a certain steady-state operating condition. Eigenvalue analysis, also known as modal analysis, is used to assess the small-signal stability [7]. The linearised model of the system can be expressed as (5).

$$\dot{\mathbf{X}} = \mathbf{Ax} + \mathbf{Bu} \tag{5}$$

In (5), **x** and **u** are state and input vectors respectively. **A** represents the state matrix and **B** is the input matrix. The *i*-th complex eigenvalue is expressed as (6). The damping ratio is an index used to determine the critical eigenvalue. The lower the damping ratio, the slower the rate of decay of oscillations associated with the eigenvalue. The calculation of the damping ratio of *i*-th eigenvalue (ζ_i) is completed as in (7).

$$\lambda_i = \sigma_i \pm j\omega_i \tag{6}$$

$$\zeta_i = \frac{-\sigma_i}{\sqrt{\sigma_i^2 + \omega_i^2}} \tag{7}$$

In (6)-(7), the subscript *i* represents *i*-th mode in the state matrix. λ is the eigenvalue of the state matrix. The real and imaginary part of the eigenvalue is represented in σ and ω respectively. For eigenvalue λ_i, the right eigenvector (ϕ_i) of **A** associated to *i*-th mode can be calculated as in (8).

$$\mathbf{A}\phi_i = \lambda_i \phi_i \tag{8}$$

In small-signal analysis, the right eigenvector, also known as the mode shape, provides information on the participation of the state variables in any selected oscillatory mode. The magnitude of a participating state in mode shape indicates the involvement of the state variable in the selected oscillatory mode. In multi-machine power systems, groups of synchronous generators associated with the inter-area oscillation can be identified by considering the relative phase difference between synchronous machine rotor speed states in the right eigenvector. The generators are classified as being within the same group if these phase differences are small [32].

4. Quantitative Measure for Mode Shape

The contribution of HVDC modelling to the damping of an inter-area oscillation varies depending on the modelling detail included and the location of any given HVDC system. Different measures can be implemented in order to quantify the errors of damping ratios of the inter-area oscillation between simplified and dynamic HVDC models. Simple error methods (such as absolute error) can be used to quantify the impact of modelling any given HVDC system in detail. However, simple error methods have low reliability and efficiency for identifying critical locations where dynamic HVDC modelling is needed. For example, the damping ratios of the inter-area oscillation with and without detailed dynamic HVDC models may be identical at one operating condition. However, when the operating condition changes, considerable differences in damping of the oscillatory mode may present as the contribution of the dynamic HVDC model is more significant at this operating point. Due to its low reliability performance, simple error measures need to be calculated for all operating scenarios – in which case full linear analysis may as well be performed.

Therefore, in this study, a new measure is developed in order to quantify changes in the critical mode shapes when simplified and dynamic HVDC modelling is used. Since the inter-area oscillation is the main focus in this research, the mode shapes of the critical inter-area oscillation need to be specified. The inter-area oscillation is first identified based on the frequency of oscillation, between 0.25–1 Hz. Then, synchronous machine rotor speeds are plotted in as a mode shape. In this study the mode shape is used to classify between the Scottish and English synchronous generators. In many commercial power system analysis software, including DIgSILENT PowerFactory or PSS/E, the

mode shapes can be directly extracted as part of the modal analysis [33], [34]. The developed index, mode shape quantification, can be used to identify locations where the dynamic models of HVDC systems can be replaced by simplified models while maintaining accuracy in results. The reliability of this developed index is significantly higher than other traditional error measures since the results are similar under all operating conditions. The calculation of the quantitative measure is explained as follows.

1. An arbitrary operating scenario is specified. Variations in system parameters can be considered if desired. In this work, three system parameters, including System Non-Synchronous Penetration (SNSP) ratio, active power generated by wind generation, and system loading, are uniformly randomly varied. The active power injected (or absorbed) by HVDC infeeds is automatically adjusted in order to obtain the target SNSP. All HVDC connections are modelled using a dynamic model representation. Modal analysis is completed and the mode shape of the critical inter-area oscillation is extracted. It will be shown in Section 6 that the selection of the operating scenario does not significantly affect the accuracy of the result.
2. Normalise the magnitudes of all vectors within the mode shape and identify the groups of synchronous generators as shown in Figure 7 (left). As inter-area oscillations are related to the oscillations between groups of generators, the speeds of synchronous generators are plotted in mode shape and the groups of generators can be identified by angular separation in mode shape. In Figure 7, blue and orange arrows represent the speed of two groups of synchronous generators.
3. Each vector is then weighted by its kinetic energy stored as shown in Figure 7 (right). The reason why energy-weighted vectors are implemented is that although the vector magnitudes in the mode shape are similar, the generator with larger kinetic energy stored has a greater contribution on inter-area oscillations than the generators with smaller kinetic energy stored.
4. Calculate a weighted average vector for each group of synchronous generators as shown in Figure 8. Each weighted average vector represents one group of generators. The calculation of the weighted average vector is expressed as (9)−(10).
5. Calculate the Euclidean distance (d) between the two weighted average vectors using (11).
6. Select a single VSC-HVDC link or a group of VSC-HVDC links to investigate the required modelling detail. Swap the dynamic VSC-HVDC model(s) for the simplified model(s) of VSC-HVDC at the target location(s).
7. Repeat steps 2−5 to produce a new value of d.
8. Compare the values of d for different cases to establish the relative importance of the different models at different locations. High values of Δd signify locations where dynamic VSC-HVDC models are likely to affect the result accuracy.

Mode shapes with post-normalised and energy-weighted vectors are shown in Figure 7. The weighted average vectors representing groups of synchronous generators oscillating against each other in an inter-area mode are shown in Figure 8.

Post-normalised mode shape

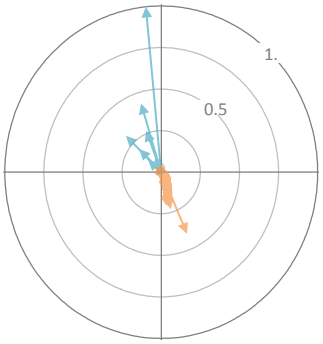

Energy-weighted mode shape

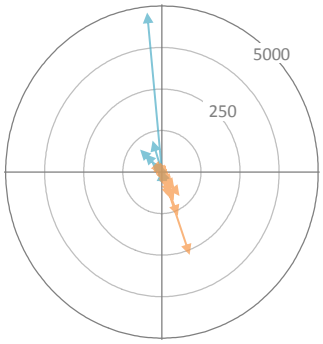

Figure 7. Mode shape with post-normalised values (left) and energy-weighted values (right)

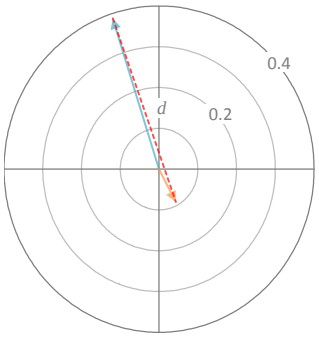

Figure 8. Mode shape representing weighted average vectors (blue and orange arrows) and Euclidean distance between two vectors (red-dashed line)

$$x_{avg} = \frac{H_1 S_1 x_1 + H_2 S_2 x_2 + \cdots + H_n S_n x_n}{H_1 S_1 + H_2 S_2 + \cdots + H_n S_n} \tag{9}$$

$$y_{avg} = \frac{H_1 S_1 y_1 + H_2 S_2 y_2 + \cdots + H_n S_n y_n}{H_1 S_1 + H_2 S_2 + \cdots + H_n S_n} \tag{10}$$

In (9)−(10), x_{avg} and y_{avg} are coordinates of the weighted average vector in x and y axis respectively. H is an inertia constant of synchronous generators. S is a total rating of synchronous generators. x and y are the coordinates of signals in a mode shape. The subscript n represents the number of generators in each group. The weighted average vectors are repeatedly computed for each group of generators. Equations (9) and (10) are developed based on the same idea as centre of inertia (COI) speed, typically used to describe the principal frequency dynamics of a power system [35]. Since the inter-area oscillations are associated with the kinetic energy stored in a group of synchronous generators, the generators' rotor speeds in the mode shape of the inter-area oscillation are decomposed in the x and y axis and the inertia constant and apparent power of each synchronous generator are used as weighting factors.

$$d = \sqrt{\left(x_{avg,1} - x_{avg,2}\right)^2 + \left(y_{avg,1} - y_{avg,2}\right)^2} \tag{11}$$

In (11), the subscript *1* and *2* represent the first and second groups of synchronous generators respectively. By comparing Euclidean distance between the systems with simplified and dynamic models, if the difference is small, there is only small impact for dynamic HVDC model on damping of the inter-area mode. Therefore, a dynamic HVDC model can be displaced by a simplified HVDC model.

5. Test System and Modelling Considerations

To assess the impact of HVDC dynamic modelling on assessment of small signal stability in power systems, a reduced order model of the future GB system is used. This model is selected as a test system as it represents a mixed AC/DC grid with a high number of HVDC connections and an inter-area oscillatory mode.

5.1. Reduced order GB system model

The model is a representative of the loading and generation scenario predicted for 2030 [36]. It consists of 29 areas and 18 HVDC systems as depicted in Figure 9. The total installed capacity of wind generation and HVDC systems in the network, obtained from Electricity Ten Year Statement (ETYS), are 40.7 GW and 23.5 GW respectively [36]–[38]. The system loads are modelled in the aggregate ZIP load model, which consists of constant impedance, constant current and constant power components as shown in (11). The ZIP load model represents the active and reactive power load as a function of voltage [7]. ZIP coefficients used in this model are selected based on Nordic Transmission System Operators (TSOs)'s choice, presented in Table 4 in the Appendix [39]. It should be noted that the aggregated ZIP model is implemented only in the system load. The simplified modelling of HVDCs is modelled as static constant power load.

Five types of synchronous generators, including nuclear, hydro, coal, CCGT and OCGT are implemented in the model. The parameters in the dynamic models of the generating units are selected from [40]. The controllers installed at the synchronous generators, both excitation and governor control systems, are selected based on IEEE recommendation [41], [42]. The static excitation system ST1A model is installed in all nuclear generators while the direct current commutator exciter DC1A is implemented in all of the remaining generating units [41]. Regarding the governor control system, CCGT and OCGT power plants use the GAST governor control system. The hydro power plants use the HYGOV governor control system and the rest of the generating units use TGOV1 [42]. Two types of wind generation are implemented, including doubly-fed induction generators (DFIG) and fully rated converters. The dynamic models of the wind generators are based on the Western Electricity Coordinating Council (WECC) generic models [43]. The summary of types of AVR and governor for different types of generation is presented in Table 5 in the Appendix.

The 29 nodes in the reduced-order future GB network are classified into four types. As presented in Figure 9, the pink and yellow dots represent nodes with two voltage levels. The pink dot consists of 132 kV and 275 kV bus bars while the yellow dot has 275 kV and 400 kV bus bars. Blue dots represent the nodes with 275 kV and purple dots denote the 400 kV nodes. The voltage levels are selected based on the substation voltages, obtained from the GB National Grid [36]. The transmission system consists of 120 transmission lines. The transmission system is separated into two voltage levels, 275 kV and 400 kV. The 275 kV branches are presented as red lines while the 400 kV branches are blue lines. Two phase shifting transformers are installed on lines 1-3 and 12-18. Full details for the test system model can be found in [44].

In the GB network, an inter-area oscillation between groups of synchronous generators in Scotland and England has existed since the late 1970s [9]. In the reduced-order GB network, the inter-area oscillation is associated with synchronous generation connected to nodes 1-10 (Scottish area) oscillating against the synchronous generation connected to nodes 11-29 (English area). The frequency of the inter-area oscillation is in the range of 0.55-0.65 Hz depending on the operating

conditions and control modes in VSC-HVDC systems. Due to a large number of wind generation and HVDC connections, the future reduced-order GB network is suitable for the studying of power system stability, especially low-frequency inter-area oscillation, in a mixed AC/DC system.

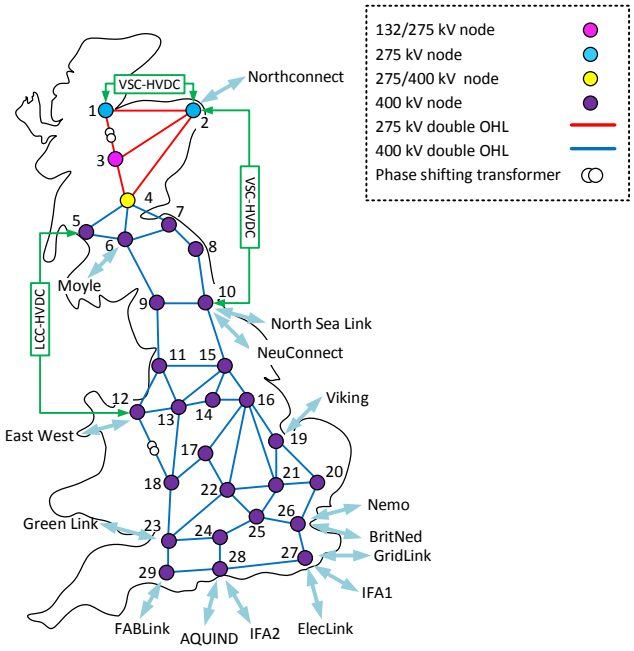

Figure 9. 29-Bus model of the future GB network with HVDC connections

5.2. Variations of Power System Operating Scenarios

In this paper, hundreds of different operating scenarios have been generated by adding variation of system variables into the grid. This includes System Non-Synchronous Penetration (SNSP) ratio, active power generated by wind generation, and system loading. The SNSP ratio is used to indicate the ratio of non-synchronous sources to system load plus power exported from HVDC [45]. The SNSP can be computed by using (12).

$$\text{SNSP} = \frac{\sum_{i=1}^{n} P_{wind} + \sum_{i=1}^{m} P_{HVDC,import}}{P_{load} + \sum_{i=1}^{p} P_{HVDC,export}} \times 100 \tag{12}$$

In (12), P_{wind} is the active power generated from wind generation. $P_{HVDC,import}$ and $P_{HVDC,export}$ are imported and exported active power through HVDC infeeds, P_{load} is the total system active power load, and n, m and p are the number of wind power plants, imported-power HVDC, and exported-power HVDC sites respectively. The maximum SNSP is defined at 75% in 2020 renewable electricity target for Ireland and Norther Ireland grid [46]. However, the maximum SNSP for the UK system has not been prescribed from the National Grid in the UK. Therefore, in this paper, the SNSP is uniformly randomly varied in the range of 0-100%.

Another system variable that has been varied is the power generated by wind generation. A correlation between wind speed and distance between UK sites was studied in [47]. However, by considering multi-variate Copulas to represent the wind speed interdependence between the 29 areas, it was found that there is no resultant correlation between wind power outputs of each of the 29 buses in the GB network. This leads to the assumption in this work that wind power outputs in 29-bus GB network are independent of each other. Wind power outputs are uniformly randomly varied from 0% to 100% of installed capacity. Lastly, system loading is set at the maximum total demand for the base

case. Both active and reactive loads at each connection point are uniformly randomly varied in the range of ±10% from the base case.

5.3. Modelling Details of HVDC in DIgSILENT PowerFactory

The simulations in this study is modelled and simulated in DIgSILENT PowerFactory 2018. Different levels of modelling fidelity have been implemented in order to identify what modelling complexity is adequate for small-signal stability studies in systems with high penetration of non-synchronous generation. Two types of HVDC modelling have been investigated in this study, including simplified HVDC modelling and dynamic HVDC modelling.

- A simplified HVDC system is modelled as a constant power load. In this model, there is no dynamic control of HVDC systems as the load can only represent the amount of active and reactive power delivered from the HVDC systems. No voltage or frequency dependence is considered within this constant power load representation.
- Dynamic modelling of a LCC-HVDC system is modelled as a twelve-pulse converter. At each end of the LCC-HVDC link, the converter is connected to two converter transformers, one with Wye-Wye and the other with Wye-Delta connections, to provide the necessary phase shifting.
- Dynamic modelling of a VSC-HVDC system is modelled based on the type of VSC-HVDC configuration – either an interconnector or an embedded link. A half-link VSC-HVDC configuration is used for all VSC-HVDC interconnector. The DC side of the VSC converter is connected to a DC voltage source. This configuration is used based on the assumption that all interconnectors are connected to strong AC grids. A full-link VSC-HVDC configuration is implemented for the embedded VSC-HVDC link since both ends of the DC transmission line are connected inside the GB network.

6. Application and Results

In this section, a large number of parameter variations are imposed on the test system in order to generate hundreds of different operating points. For the same operating scenarios, the HVDC models are switched between simplified and dynamic modelling. The damping ratios of the inter-area mode are compared for cases with different levels of modelling detail and when operating with different control systems in order to investigate the impacts on power system small signal stability. The subsets of studies are explained as follows.

1. VSC-HVDC *P*-*Q* Control: all of the HVDC infeeds are modelled in *P*-*Q* control mode. In embedded HVDC links, the V_{dc}-*Q* and *P*-*Q* control modes are implemented at the rectifier and inverter sides respectively.
2. VSC-HVDC *P*-V_{ac} Control: the dynamic models of the VSC-HVDC systems are the same as the case study above except for the control strategies. In this study, the control mode for infeeds is changed from *P*-*Q* control to *P*-V_{ac} control.

In all studies, the control strategies of LCC-HVDC systems are modelled as explained in Section 2. The impacts of different modelling fidelities and control approaches on small-signal stability are first investigated through modal analysis. Two operating scenarios are selected from the 300 generated operating scenarios. The eigenvalues of the inter-area oscillation with different fidelities of HVDC modelling are plotted in Figure 10 and Figure 11. The blue-shaded circle represents the same inter-

area oscillation with different levels of HVDC modelling. The results show that in the first selected operating scenario in Figure 10 there are only very minor differences between the eigenvalues of the inter-area oscillation under the systems with simplified and dynamic HVDC modelling. However, in the second operating scenario in Figure 11, a significant difference in eigenvalues results is found depending on modelling fidelity when the P-V_{ac} control is implemented. The eigenvalue of the inter-area oscillation in the system with P-V_{ac} control moves further towards the left-half plane while the eigenvalues of the other two cases are almost identical. By comparing the movements of the eigenvalues in these two plots, it is obvious that impacts of different HVDC modelling fidelity on the eigenvalues of the inter-area oscillation change under different operating conditions. However, it is not practicable to analyse the differences in the eigenvalue results for all operating scenarios one by one using plots of the complex plane. Instead, the damping ratios of the inter-area oscillation with different fidelities of HVDC modelling are directly compared.

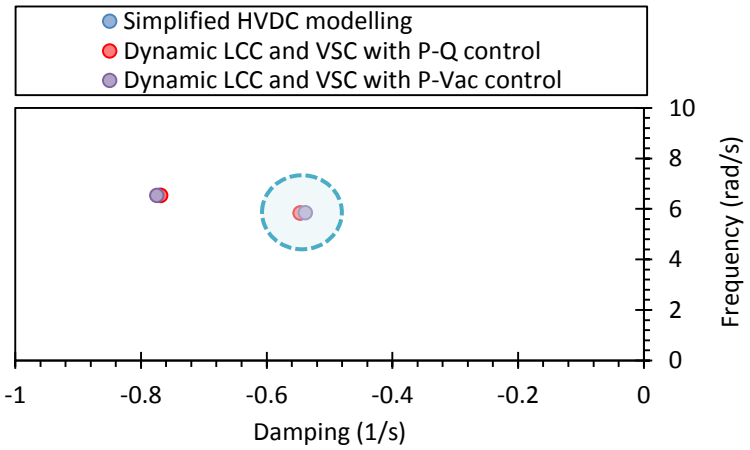

Figure 10. Eigenvalues of the inter-area mode under different levels of HVDC modelling (first operating condition representing small changes in eigenvalues)

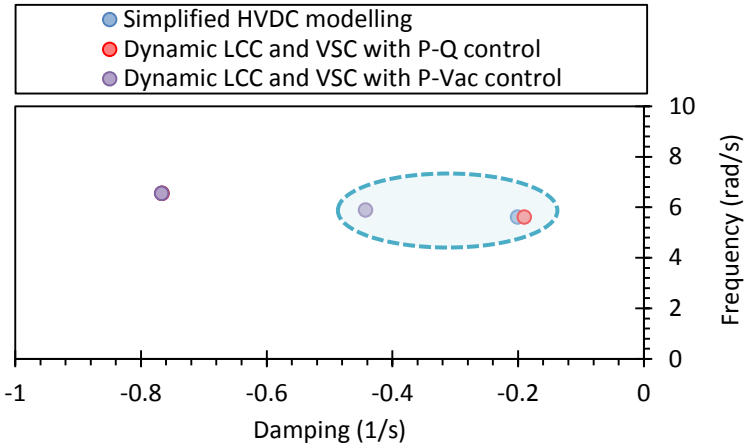

Figure 11. Eigenvalues of the inter-area mode under different levels of HVDC modelling (second operating condition representing significant changes in eigenvalues)

6.1. Identifying Priority Locations for Dynamic HVDC Modelling using Mode Shape

As presented in Figure 10 and Figure 11, the errors of damping of the inter-area oscillation under different modelling details are varied with operating scenarios. The index, called mode shape quantification, is presented since the impacts of different HVDC modelling on the mode shapes are relatively unchanged under different operating conditions. One operating scenario is randomly

selected to identify the priority locations for detailed modelling. Then, the mode shape differences are calculated when different HVDC models are switched between simplified and dynamic models. This is completed for different VSC-HVDC outer control schemes, both P-V_{ac} and P-Q control modes. Prior to the calculations of mode shape quantification, the impacts of different control approaches on the mode shape of the inter-area mode are investigated. Different control approaches in Eastern link are tested as an example. The mode shapes representing weighted average vectors for the system with simplified and dynamic VSC-HVDC with P-Q control of Eastern link are presented in Figure 12. It is clear that there is no discernible difference between the mode shapes of the system between the cases with simplified and dynamic modelling of Eastern link when the P-Q control is implemented. The two mode shapes are perfectly aligned with each other. The comparison between mode shapes for the cases with simplified and dynamic VSC-HVDC with P-V_{ac} control of Eastern link is presented in Figure 13. In this case, the angle of weighted average vectors for the Scottish generators increases, resulting in increasing angle differences between the vectors representing two groups of generators.

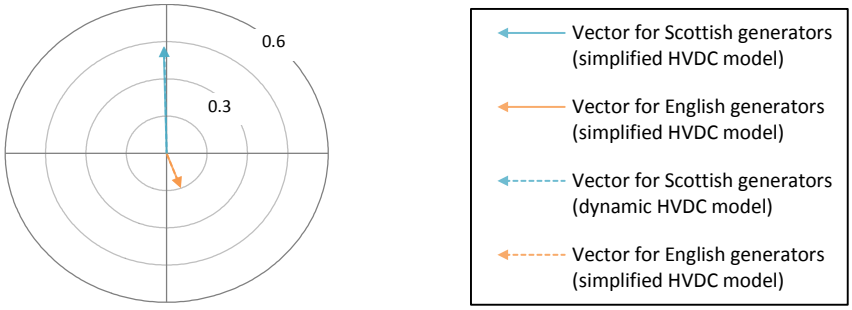

Figure 12. Mode shapes representing weighted average vectors of Scottish and English generators, comparing between simplified and dynamic VSC-HVDC with P-Q control of Eastern link

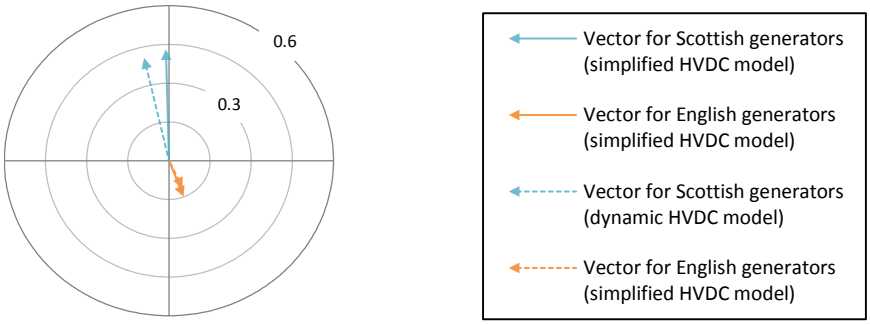

Figure 13. Mode shapes representing weighted average vectors of Scottish and English generators, comparing between simplified and dynamic VSC-HVDC with P-V_{ac} control of Eastern link

In Figure 14, the differences between mode shapes (Δd) are computed as explained in Section 4. The bar chart represents two main aspects of the comparisons of mode shape differences, which are types and locations of HVDC systems. It should be noted that there is only one control strategy in LCC-HVDC. Therefore, there is only one column representing changes in mode shapes of each LCC-HVDC.

The mode shape differences between simplified and dynamic models of VSC-HVDC with P-V_{ac} control are represented in the green-shaded bars in Figure 14. The top row in the bar chart shows the changes in mode shapes when dynamic models of all LCC-HVDC and VSC-HVDC are connected. As

shown in Figure 14, it is apparent that the largest change in mode shapes appears when dynamic models of VSC-HVDC with P-V_{ac} control are connected to the system at all locations.

The green-shaded bars from the second to sixth rows show the mode shape differences when a dynamic model of the VSC-HVDC systems in Scotland is connected one at a time. As shown in Figure 14, the changes are less significant when one of the VSC-HVDC systems with P-V_{ac} control is connected to the Scottish area, compared to the previous case. However, the magnitudes of the mode shape differences are still significant, compared to the cases of a dynamic model of an HVDC system connected to England.

The other rows illustrate the changes in mode shapes when a dynamic model of single HVDC system is connected to England one at a time. It is obvious that there is no significant change in mode shape differences when a dynamic model of VSC-HVDC with P-V_{ac} control is connected to England.

By comparing the magnitudes of mode shape differences, although the most accurate result is obtained when the dynamic VSC-HVDC models with P-V_{ac} control are connected to all locations in the system, the main contribution on the damping of the inter-area oscillation is from the dynamic VSC-HVDC models in Scotland. Therefore, the dynamic VSC-HVDC models with P-V_{ac} control are required to connect to Scotland in order to maintain the accuracy in the results while the others connected to England can be connected by using simplified model.

The mode shape differences of dynamic models of LCC-HVDC and VSC-HVDC with P-Q control are presented in red-shaded bars. The results show that there are only slight changes found when the dynamic models of LCC-HVDC and VSC-HVDC with P-Q control are connected. Therefore, from the results in Figure 14, the dynamic models of LCC-HVDC and VSC-HVDC with P-Q control can be replaced by the simplified model of a static, constant power, load.

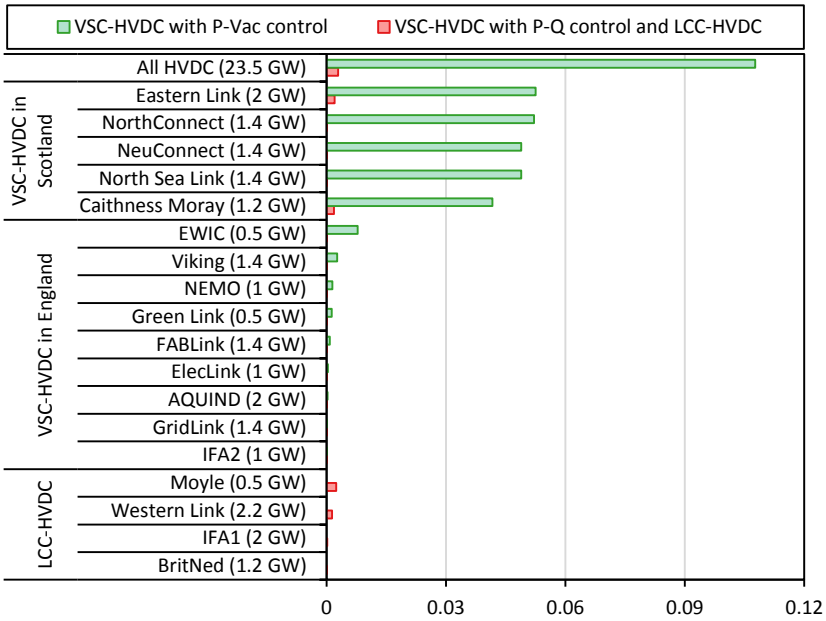

Figure 14. Mode shape quantification

The parameters of both LCC-HVDC and VSC-HVDC are presented in Table 6 and Table 7 in the Appendix respectively. The rating of each HVDC is presented in Figure 14. The parameters settings for different control approaches are shown in Table 8-Table 11 in the Appendix. It should be noted

that the rated power of the HVDC is not presented in the tables since each HVDC system has different power rating. The per-unit values are calculated based on the rated values of individual HVDC.

6.2. VSC-HVDC P-Q Control

Damping ratios of the inter-area oscillation between the systems with simplified and dynamic HVDC modelling are plotted in Figure 15. The results show that points are closely aligned with the identity line (which would represent identical results). It should be noted that the percentage is the unit of the damping ratio, which does not indicate a relative difference to any measures. Consequently, in order to avoid unnecessary model complexity and reduce computational burden in simulations, the simplified model can be used in the small-signal stability study instead of implementing dynamic model of either LCC-HVDC or VSC-HVDC with *P-Q* control.

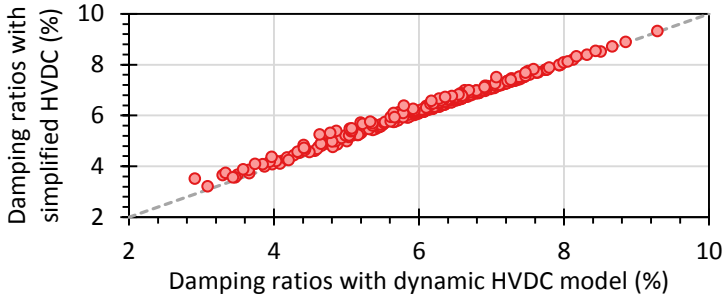

Figure 15. Damping ratios between the system with all simplified HVDC modelling (y-axis) and all dynamic HVDC modelling (x-axis)

One operating scenario is randomly selected and the mode shape differences are quantified. The changes in mode shapes are then plotted against the mean absolute deviation of damping ratios (ζ_{MAD}) as shown in Figure 16. This mean absolute deviation is computed by averaging the absolute difference between damping ratios of the system simplified and dynamic models across all operating points. The mean deviation in the damping ratio determined using simplified HVDC models at all locations is only 0.091%. It is obvious that the dynamic models of LCC-HVDC and VSC-HVDC with *P-Q* control do not have any significant impact on the critical eigenvalue mode shape or the damping ratio of the inter-area oscillation.

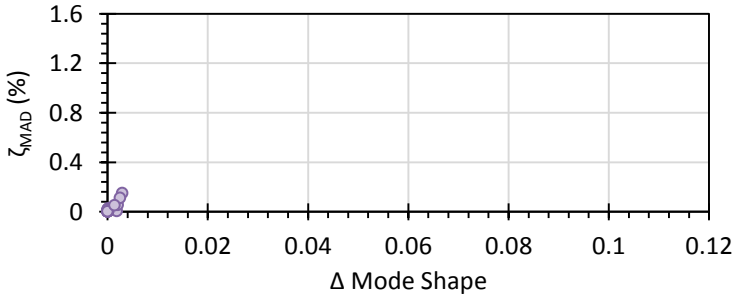

Figure 16. Mode shape differences between the systems with simplified and dynamic HVDC models. Axes are scaled to be comparative with similar plots later in the paper to emphasize the result.

With dynamic HVDC modelling at all locations, the simulation for modal analysis in DIgSILENT requires approximately 3 minutes and 15 seconds. However, when all dynamic HVDC modelling is replaced by the simplified HVDC modelling, the simulation for modal analysis is completed within 1 minute and 50 seconds, 43.59% faster than the system with dynamic HVDC modelling at all locations.

6.3. VSC-HVDC P-V_{ac} Control

The damping ratios between the simplified and dynamic HVDC models are illustrated in Figure 17. In this plot, it is apparent that there is no significant difference in damping ratios when the AQUIND interconnector is modelled as a dynamic VSC-HVDC model with *P*-V_{ac} control. The AQUIND link is shown as an example in Figure 17 but similar results are obtained when any of the England-connected VSC-HVDC infeed links are considered. Conversely, the damping ratios start deviating from the identity line when a dynamic model of the VSC-HVDC system is modelled for NorthConnect. Here, NorthConnect is used as an illustrative example for Scotland-connected VSC-HVDC systems. Lastly, there are significant deviations when all dynamic HVDCs are connected.

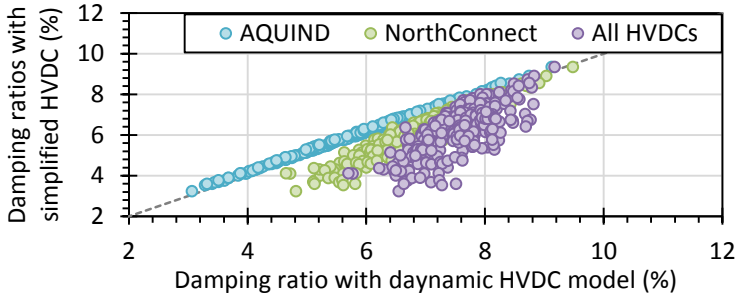

Figure 17. Damping ratios between the system with all simplified HVDC modelling (y-axis) and dynamic HVDC modelling (x-axis)

As shown in Figure 17, neglecting the dynamics of the VSC-HVDC model with *P*-V_{ac} control for NorthConnect (in Scotland) leads to a significant deviation from the identity line and errors in the modal analysis. This situation results from a significant lack of reactive power reserve in the Scottish area. The total installed capacity of the synchronous generators in England is approximately ten times larger than the installed capacity of the synchronous generators in Scotland. Therefore, when perturbed, reactive power support is required from the Scottish VSC-HVDCs to regulate the voltages at all Scottish buses. However, the reactive power reserve from synchronous generators in England is large enough to support the English network. Therefore, capturing the AC voltage support action of the VSC-HVDCs in England is less critical.

In order to support this line of argument and enable greater generalisation of the results, the following simulation experiment has been performed. Static VAr Compensators (SVCs) are added into the Scottish area in order to provide reactive power support. The total additional installed capacity of the SVCs is equal to the total installed capacity of the Scottish VSC-HVDCs. The rating of SVCs at each node is equally distributed over all Scottish buses (Nodes 1−10). The steady-state operating condition remains identical to the operation before connecting the SVCs since there is no reactive power injection from SVCs during steady-state operation, only following perturbations. Then, the simplified and dynamic VSC-HVDC model with *P*-V_{ac} control is compared at a randomly selected operating condition. The results show that, in the system with additional Scottish SVCs connected, the damping ratios of the inter-area oscillation between simplified and dynamic VSC-HVDC model with *P*-V_{ac} control ($\Delta\zeta$) is almost identical and the mode shape differences (Δd) becomes smaller as shown in Table 2. With this new addition of reactive power support, the index Δd is reduced and indicates that these VSC-HVDC links (even with *P*-V_{ac} control) can be replaced by static, constant power, loads without significantly introducing error into the results.

Table 2: Mode shape differences and damping ratios of the inter-area mode before and after connecting additional SVCs in Scotland

	Without additional SVCs	With additional SVCs
Mode shape differences (Δd)	0.108	0.000824
Damping ratio differences ($\Delta\zeta$)	3.766%	0.067%

The reliability of the mode shape quantification is then investigated. Three different scenarios are randomly selected, including large damping ratio difference (red-shaded area), medium damping ratio difference (blue-shaded area) and small damping ratio difference (orange-shaded area). These operating scenarios are selected to illustrate how the change in mode shape metric can be used to identify critical HVDC converters which require dynamic models independently of the selected operating point. The mean absolute deviation of damping ratios is computed separately for every model change. The changes in mode shapes in three scenarios are quantified and plotted against the mean absolute deviation of damping ratios as shown in Figure 18.

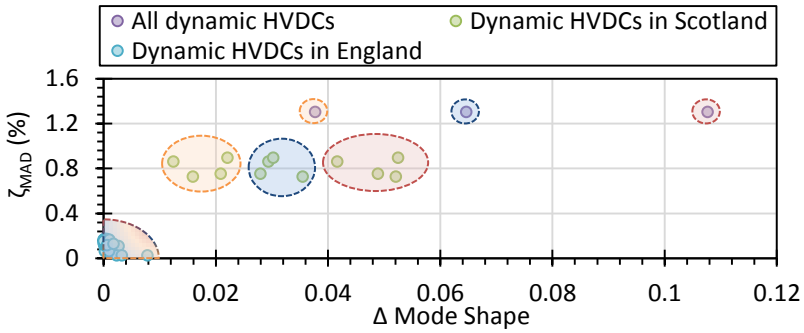

Figure 18. Mode shape differences at different operating points

According to Figure 18, it is apparent that the mean absolute deviations of damping ratios are significant when a dynamic VSC-HVDC is connected to Scotland one at a time and when all dynamic HVDCs are connected to the system. However, there are only slight differences in damping ratios in all operating points when an England-connected HVDC is modelled with all dynamics (bottom left). The plots also show that although the magnitudes of mode shape differences vary over three different scenarios, they are able to separate the cases with large damping deviations from the cases with small damping deviations. This separation, however, cannot be obviously identified when a simple error measure, such as percentage error, is implemented. The operating scenario with a small damping ratio difference is selected in order to show the reliability of the percentage error as a predictor of required modelling detail. In this study, the percent error is the ratio of the absolute damping ratio differences between simplified and dynamic HVDC modelling to the damping ratio of dynamic HVDC modelling. As presented in Figure 19, unlike mode shape differences, there is no clear separation between the locations that require dynamic HVDC modelling and the locations that do not need to implement the dynamic HVDC modelling.

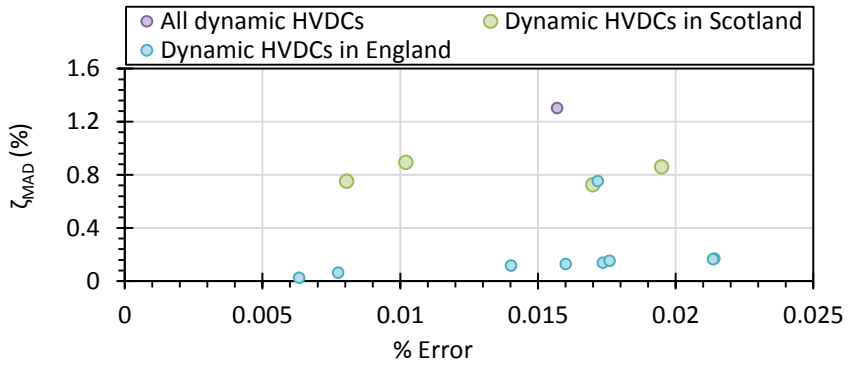

Figure 19. Percent errors between simplified and dynamic HVDC modelling at different locations

As shown in Figure 20, the system with Scotland-connected dynamic HVDC model can achieve almost identical damping ratios to the system with dynamic models at all locations. The mean absolute deviation of damping ratios is only 0.32%. The relationship is highly linear and very consistent across all values of damping ratio (compared, for example, to Figure 17). Therefore, this index, representing mode shape differences, can be used to identify the locations in large-scale power systems where a dynamic HVDC model can be replaced by simplified model to reduce the model complexity and computational burden in simulation while maintaining the accuracy of the results.

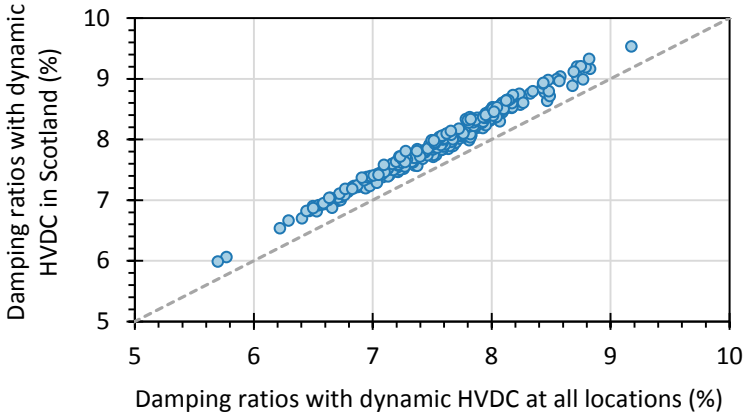

Figure 20. Damping ratios between the system with Scotland-connected dynamic HVDC (y-axis) and all dynamic HVDC modelling (x-axis)

By replacing all of the dynamic VSC-HVDC models in England and the dynamic LCC-HVDC models to the simplified HVDC model, the simulation time of the modal analysis reduces to 2 minutes, which is approximately 40% faster than the simulation on the system with dynamic HVDC modelling at all locations.

The simulation times of modal analysis between different model fidelities are presented in Table 3. The results show that after replacing the dynamic HVDC models with the simplified HVDC model (where possible), the simulation time in both study cases reduces approximately 40% from the system with dynamic HVDC modelling at all locations while the accuracy of small-signal stability results is maintained.

Table 3: Comparisons of simulation times under different levels of modelling fidelity

Study case	HVDC modelling fidelity	Simulation time (s)
LCC-HVDC and VSC-HVDC with *P*-*Q* Control	Dynamic HVDC models at all locations	195
	Simplified HVDC models at all locations	110
VSC-HVDC with *P*-V_{ac} Control	Dynamic HVDC models at all locations	200
	Simplified HVDC models in England	120

6.4. Reliability of Mode Shape Quantification on Variations in Grid Topology

Damping of inter-area oscillations can be influenced by the network topology, power flows or the fast excitation systems. Low-frequency inter-area oscillations are therefore sensitive to variations in a network topology. To investigate the reliability of the developed index on the changing network structure, one of the major tie lines, connected between nodes 10 and 15, is tripped, representing changes in the system structure. The quantitative measure for mode shape is calculated under new network topology. The results in Figure 21 show that the dynamic VSC-HVDC modelling with *P*-V_{ac} control is required to install in the system in order to maintain the accuracy of the small-signal stability results.

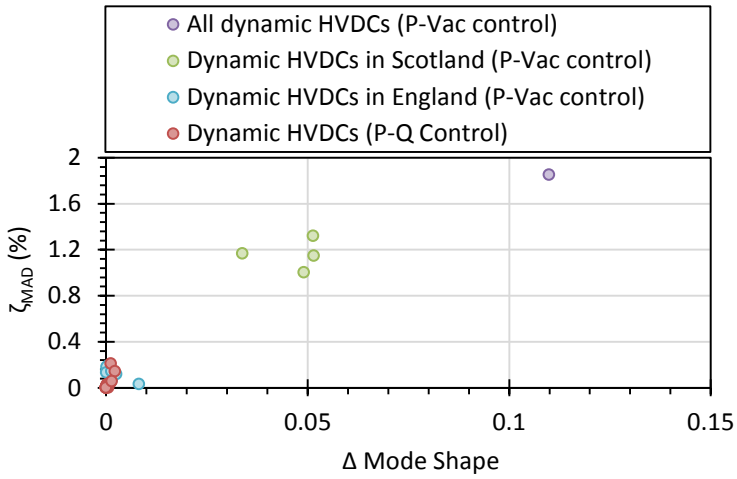

Figure 21. Mode shape differences in the changing network structure

In order to support the results in Figure 21, damping ratios of the inter-area oscillation between the systems with simplified and dynamic HVDC modelling are compared in Figure 22 and Figure 23. As illustrated in Figure 21, the values of mode shape differences for the dynamic models of LCC-HVDC and VSC-HVDC with *P*-*Q* control is significantly low. Therefore, the dynamic modelling of these HVDC systems can be replaced by the simplified HVDC model. The results in Figure 22 show that, under the changed network topology, the damping ratios of the critical inter-area oscillation between the system with simplified HVDC modelling and the system with dynamic LCC-HVDC and VSC-HVDC with *P*-*Q* control are almost identical.

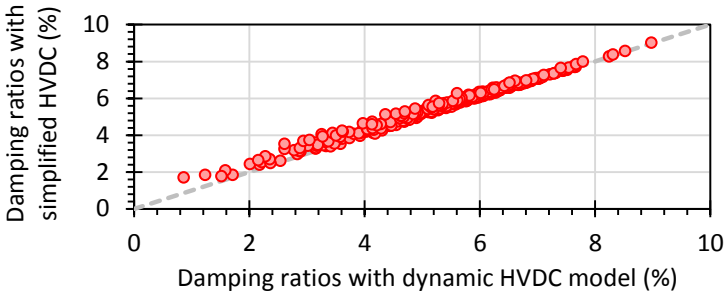

Figure 22. Damping ratios between the system with all simplified HVDC modelling (y-axis) and all dynamic HVDC modelling (x-axis) in the changing network structure

According to Figure 21, the dynamic model of VSC-HVDC with P-V_{ac} control in Scotland is required to install in the system in order to maintain the accuracy of the small-signal stability results. All of the HVDC connections except VSC-HVDC with P-V_{ac} control in Scotland are replaced by the simplified HVDC modelling. The results in Figure 23 show that the damping ratios of the inter-area oscillation between the system with all dynamic HVDC modelling and the system with dynamic VSC-HVDC with P-V_{ac} control only in Scotland are almost similar. Based on these simulations, it can be conclude that although the network topology has been changed, the quantitative indices are still able to separate the groups of HVDC that can be replaced by simplified HVDC modelling.

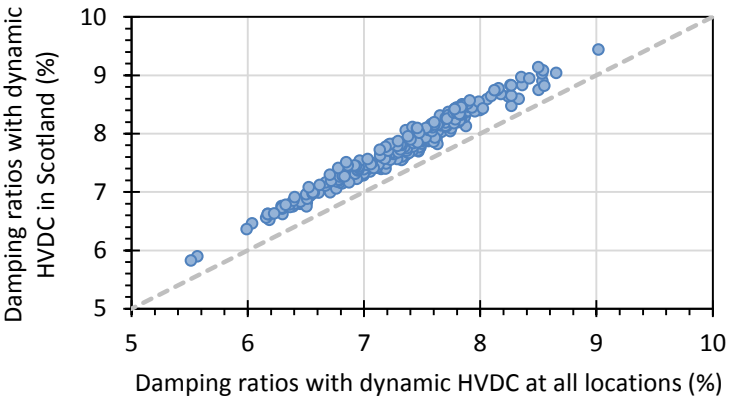

Figure 23. Damping ratios between the system with Scotland-connected dynamic HVDC (y-axis) and all dynamic HVDC modelling (x-axis) in the changing network structure

7. Conclusions

Due to a significant integration of HVDC systems, studies of power system stability in large-scale mixed AC/DC systems are required. The dynamic modelling of HVDC can achieve the most accurate dynamic responses but computationally expensive simulations and high levels of modelling skill are required. A simplified model, however, is easy to implement but it will neglect some dynamic characteristics of the devices, possibly resulting in inaccuracy of the results. A new measure is developed in this study to identify which dynamic HVDC systems should be modelled in order to maintain the accuracy of small-signal stability results.

The illustrative study shows that relative small changes in mode shapes also indicate little differences in damping ratios between the different fidelity of models used. For example, all the dynamic models of LCC-HVDC and VSC-HVDC with P-Q control can be neglected in small-signal stability assessment as there is no significant change in the results. Furthermore, this index can be used to indicate the locations where dynamic models are needed. The results show that, by replacing

the dynamic HVDC model at the targeted locations (Scotland-connected VSC-HVDC), the system can achieve almost identical results compared to the system with dynamic models at all locations with less computational burden and reduced complexity in the system modelling.

The proposed index is calculated with changing network structure in order to investigate the performance of the mode shape quantification under different grid topology. One of the tie lines originally connected between the areas is removed from the network in order to make a significant change in the inter-area oscillation. The results show that although the structure of the test system has been changed, the proposed index is still able to identify the locations where dynamic models are needed. Therefore, the mode shape quantification approach proposed is not grid topology sensitive.

In this study, the capability of the proposed index for identifying the locations that require dynamic HVDC modelling has been proven through the numerical results. In order to prove the generality of this conclusion, modal sensitivity analysis could be conducted as a possible extension of the work. Furthermore, as in Figure 18, the index shows the obvious separation between the locations where the dynamic HVDC modelling is required and the locations where the simplified HVDC modelling can be used. Future research could be conducted to define a suitable threshold to identify where the simplified HVDC modelling can be implemented without reducing the accuracy of the small-signal stability results.

8. Appendix

Table 4: ZIP parameters used in the future GB network model

	Z_p	I_p	P_p	Z_q	I_q	P_q
ZIP coefficients	0.4	0.0	0.6	0.9	0.0	0.1

Table 5: Types of AVR and Governor for generators in the GB system

Generation Types	AVR Types	Governor Types
Coal	DC1A	TGOV1
CCGT	DC1A	GAST
OCGT	DC1A	GAST
Hydro	DC1A	HYGOV
Nuclear	ST1A	TGOV1

Table 6: Parameters of LCC-HVDC system

Parameters	Values
Rated AC voltage	551 kV
Rated DC voltage	1000 kV
Arm resistance	0.006 Ω
Arm inductance	60 mH
Number of submodules per arm	200
Submodule capacitance	10000 μF

Table 7: Parameters of VSC-HVDC system

Parameters	Values
Rated AC voltage	400 kV
Rated DC voltage	600 kV
Number of bridges in series	2
DC line resistance	1
Commutation resistance per bridge	0.05 Ω
DC line inductance	1200 mH

Table 8: Parameters in *P*-*Q* control mode of VSC-HVDC

Parameters	Values
Proportional gain for active power control	2
Integral gain for active power control	40
Proportional gain for reactive power control	1
Integral gain for reactive power control	100

Table 9: Parameters in P-V_{ac} control mode of VSC-HVDC

Parameters	Values
Proportional gain for active power control	2
Integral gain for active power control	40
Proportional gain for AC voltage control	12
Integral gain for AC voltage control	100

Table 10: Parameters in V_{dc}-Q control mode of VSC-HVDC

Parameters	Values
Proportional gain for DC voltage control	7
Integral gain for DC voltage control	120
Proportional gain for reactive power control	1
Integral gain for reactive power control	40

Table 11: Parameters in current control, voltage control, and gamma control in LCC-HVDC

Parameters	Values
DC current transducer time constant	0.05 s
DC voltage transducer time constant	0.05 s
Minimum DC voltage following blocking	10 kV
Minimum DC current following blocking	10 A
Rectifier AC blocking voltage	0.7 p.u.
Inverter DC bypassing voltage	0.7 p.u.
Rectifier AC unblocking voltage	0.8 p.u.
Inverter DC bypassing voltage	0.8 p.u.
Minimum blocking time	0.2 s
Minimum bypassing time	0.4 s
Inverter current reference margin	0.1 p.u.
Proportional gain in voltage control	2 p.u.
Integral time constant in voltage control	0.02 s
Proportional gain in current control	1 p.u.
Integral time constant in current control	0.02 s
Proportional gain in gamma control	0.1 p.u.
Integral time constant in gamma control	0.1 s

9. References

[1] European Commission, "Renewable energy Moving towards a low carbon economy," 2018. [Online]. Available: https://ec.europa.eu/energy/en/topics/renewable-energy. [Accessed: 07-Mar-2019].

[2] GreenMatch, "Renewable Energy in the United Kingdom," 2019. [Online]. Available: https://www.greenmatch.co.uk/blog/2018/03/renewable-energy-in-the-united-kingdom. [Accessed: 05-Mar-2019].

[3] Department for Business Energy & Industrial Strategy, "Industrial Strategy Offshore Wind Sector Deal," Mar. 2019.

[4] International Energy Agency, "Large-scale electricity interconnection - Technology and prospects for cross-regional networks," 2016.

[5] W. Gene and A. Ram, "2017 Was A Fantastic Year For HVDC Technologies," 2018. [Online]. Available: https://www.tdworld.com/hvdc/2017-was-fantastic-year-hvdc-technologies. [Accessed: 11-Mar-2019].

[6] M. R. Shah, J. Sanchez, R. Preece, and M. Barnes, "Stability and Control of Mixed AC-DC Systems with VSC-HVDC: A Review," *IET Gener. Transm. Distrib.*, pp. 1–15, Jan. 2018.

[7] P. Kundur, N. J. Balu, and M. G. Lauby, *Power System Stability and Control*. McGraw-Hill Education, 1994.

[8] A. Atputharajah and T. K. Saha, "Power system blackouts - literature review," in *2009 International Conference on Industrial and Information Systems (ICIIS)*, 2009, pp. 460–465.

[9] H. Wang and W. Du, *Analysis and Damping Control of Power System Low-frequency Oscillations*. Boston, MA: Springer US, 2016.

[10] A. K. Pathak, M. P. Sharma, and M. Gupta, "Effect on static and dynamic reactive power in high penetration wind power system with altering SVC location," in *2016 IEEE 6th International Conference on Power Systems (ICPS)*, 2016, pp. 1–6.

[11] I. Norheim, O. Mogstad, C. Jauch, P. Sørensen, D. Pudjianto, and O. Anaya-lara, "Case Studies on System Stability with Increased RES-E Grid Integration," 2005.

[12] T. Skånøy, “Steady-state and dynamic converter modeling in system analysis,” Norwegian University of Science and Technology, 2007.

[13] M. Imhof and G. Andersson, “Dynamic modeling of a VSC-HVDC converter,” in *2013 48th International Universities’ Power Engineering Conference (UPEC)*, 2013, no. Vsc 2, pp. 1–6.

[14] W. Du, Q. Fu, and H. Wang, “Comparing AC Dynamic Transients Propagated Through VSC HVDC Connection With Master–Slave Control Versus DC Voltage Droop Control,” *IEEE Trans. Sustain. Energy*, vol. 9, no. 3, pp. 1285–1297, Jul. 2018.

[15] H. Atighechi *et al.*, “Dynamic Average-Value Modeling of CIGRE HVDC Benchmark System,” *IEEE Trans. Power Deliv.*, vol. 29, no. 5, pp. 2046–2054, Oct. 2014.

[16] A. Zheng, C. Guo, P. Cui, W. Jiang, and C. Zhao, “Comparative Study on Small-Signal Stability of LCC-HVDC System With Different Control Strategies at the Inverter Station,” *IEEE Access*, vol. 7, pp. 34946–34953, 2019.

[17] Y. Wang, C. Zhao, and C. Guo, “Comparison study of small-signal stability of MMC-HVDC system in different control modes,” *Int. J. Electr. Power Energy Syst.*, vol. 111, no. August 2018, pp. 425–435, Oct. 2019.

[18] G. Grdenic, M. Delimar, and J. Beerten, “Comparative Analysis on Small-Signal Stability of Multi-Infeed VSC HVDC System With Different Reactive Power Control Strategies,” *IEEE Access*, vol. 7, pp. 151724–151732, 2019.

[19] C. Guo, W. Liu, J. Zhao, and C. Zhao, “Impact of control system on small-signal stability of hybrid multi-infeed HVDC system,” *IET Gener. Transm. Distrib.*, vol. 12, no. 19, pp. 4233–4239, 2018.

[20] D. Jovcic and K. Ahmed, *High Voltage Direct Current Transmission: Converters, Systems and DC Grids*. Wiley, 2015.

[21] CIGRE Working Group B4-57, “Guide for the development of models for HVDC converters in a HVDC grid,” 2014.

[22] A. Jamshidi Far and D. Jovcic, “Small-Signal Dynamic DQ Model of Modular Multilevel Converter for System Studies,” *IEEE Trans. Power Deliv.*, vol. 31, no. 1, pp. 191–199, Feb. 2016.

[23] Siemens Energy Inc., “PSS/E 32.0 Model Library.” Siemens Energy Inc.: Schenectady, NY, USA, 2009.

[24] P. W. Sauer, M. A. Pai, and J. H. Chow, *Power System Dynamics and Stability: With Synchrophasor Measurement and Power System Toolbox 2e*. Chichester, UK: John Wiley & Sons, Ltd, 2017.

[25] Å. M. Halvorsdatter, “HVDC Transmission Using a Bipolar Configuration Composed of an LCC and MMC,” Norwegian University of Science and Technology, 2014.

[26] J. Arrillaga and B. D. Smith, *AC-DC power system analysis*. Stevenage: Institution of Electrical Engineers, 1998.

[27] M. Eremia, C. Liu, and A. Edris, *Advanced Solutions in Power Systems: HVDC, FACTS, and Artificial Intelligence*. Hoboken, NJ, USA: John Wiley & Sons, Inc., 2016.

[28] C. Hahn, A. Semerow, M. Luther, and O. Ruhle, “Generic modeling of a line commutated HVDC system for power system stability studies,” in *2014 IEEE PES T&D Conference and Exposition*, 2014, pp. 1–6.

[29] A. Beddard and M. Barnes, “Modelling of MMC-HVDC Systems – An Overview,” *Energy Procedia*, vol. 80, pp. 201–212, 2015.

[30] A. Beddard, M. Barnes, and R. Preece, “Comparison of Detailed Modeling Techniques for MMC Employed on VSC-HVDC Schemes,” *IEEE Trans. Power Deliv.*, vol. 30, no. 2, pp. 579–589, Apr. 2015.

[31] P. Kundur *et al.*, “Definition and Classification of Power System Stability IEEE/CIGRE Joint Task Force on Stability Terms and Definitions,” *IEEE Trans. Power Syst.*, vol. 19, no. 3, pp. 1387–1401, Aug. 2004.

[32] A. K. Singh and B. C. Pal, “Chapter 2 - Power System Modeling, Simulation, and Control Design,” in *Dynamic Estimation and Control of Power Systems*, A. K. Singh and B. C. Pal, Eds. Academic Press, 2019, pp. 9–33.

[33] Siemens AG 2017, “Small Signal Stability Analysis Module Network Eigenvalue Analysis for PSS®E.” [Online]. Available: http://descargas.indielec.com/web/Module Small Signal Stability Analysis PSSE.pdf. [Accessed: 16-Apr-2020].

[34] *User Manual - Technical References of Models*. DIgSILENT PowerFactory, 2018.

[35] J. Schiffer, P. Aristidou, and R. Ortega, “Online Estimation of Power System Inertia Using Dynamic Regressor Extension and Mixing,” *IEEE Trans. Power Syst.*, vol. 34, no. 6, pp. 4993–5001, Nov. 2019.

[36] “Electricity Ten Year Statement (ETYS),” *National Grid*. [Online]. Available: https://www.nationalgrid.com/uk/publications/electricity-ten-year-statement-etys. [Accessed: 13-Mar-2018].

[37] M. Barnes, “VSC-HVDC Newsletter,” *School of Electrical & Electronic Engineering, University of Manchester*, vol. 4, no. 12, pp. 1–9, 2017.

[38] “Interconnectors,” 2018. [Online]. Available: https://www.4coffshore.com/transmission/interconnectors.aspx. [Accessed: 07-Aug-2018].

[39] A. Perez Tellez, “Modelling aggregate loads in power systems,” KTH ROYAL INSTITUTE OF TECHNOLOGY, 2017.

[40] P. M. Anderson and A. A. Fouad, *POWER SYSTEM CONTROL AND STABILITY, 2ND ED*. Wiley India Pvt. Limited, 2008.

[41] PES, *IEEE Recommended Practice for Excitation System Models for Power System Stability Studies*, vol. 2005, no. April. 2006.

[42] IEEE Power & Energy Society, “Dynamic Models for Turbine-Governors in Power System Studies,” 2013.

[43] P. Pourbeik *et al.*, “Generic stability models for type 3 & 4ind turbine generators for WECC,” in *2013 IEEE Power & Energy Society General Meeting*, 2013, pp. 1–5.

[44] S. Asvapoositkul and R. Preece, “Analysis of the variables influencing inter-area oscillations in the future Great Britain power system,” in *15th IET International Conference on AC and DC Power Transmission (ACDC 2019)*, 2019, pp. 1–7.

[45] J. O’Sullivan, A. Rogers, D. Flynn, P. Smith, A. Mullane, and M. O’Malley, “Studying the Maximum Instantaneous Non-Synchronous Generation in an Island System—Frequency Stability Challenges in Ireland,” *IEEE Trans. Power Syst.*, vol. 29, no. 6, pp. 2943–2951, Nov. 2014.

[46] EirGrid, SEMO, and SONI, “The DS3 Programme Delivering a Secure, Sustainable Electricity System,” 2015. [Online]. Available: http://www.eirgridgroup.com/site-files/library/EirGrid/DS3-Programme-Brochure.pdf. [Accessed: 08-Mar-2019].

[47] G. Sinden, “Characteristics of the UK wind resource: Long-term patterns and relationship to electricity demand,” *Energy Policy*, vol. 35, no. 1, pp. 112–127, Jan. 2007.